7-31-2015

Using Stochastic Differential Equations to Model Gap-Junction Gating Dynamics in Cardiac Myocytes

Will Consagra

Using Stochastic Differential Equations to Model Gap-Junction Gating Dynamics in Cardiac Myocytes

by

Will Consagra

A Thesis Submitted in Partial Fulfillment of the Requirements
for the Degree of Master of Science in Applied Mathematics
School of Mathematical Sciences, College of Science

Rochester Institute of Technology
Rochester, NY

July 31, 2015

Committee Approval:

R·I·T
College of
SCIENCE

Dr. Elizabeth Cherry Date

School of Mathematical Sciences

Thesis Advisor

Dr. Seshavadhani Kumar Date

School of Mathematical Sciences

Committee Member

Dr. Laura Munoz Date

School of Mathematical Sciences

Committee Member

Nathan Cahill, D.Phil. Date

School of Mathematical Sciences

Director of Graduate Programs

Abstract

The cell-to-cell propagation of the cardiac action potential allows for the electro-mechanical coupling of cells, which promotes the coordinated contraction of cardiac tissue, often referred to as the heartbeat. The main structures that promote electrical coupling between adjacent cardiac cells are pore-like proteins called gap junctions that line the membranes of such cells, allowing a channel for electrically charged ions to travel between cells. It is known that the conformational, and hence conducting, properties of gap-junction channels change as a function of local gap-junctional voltage and local ionic concentrations and are stochastic in nature. Many previous models of gap junctions have made a constant-resistance approximation or used an ODE model relating gating state to a local voltage. In this thesis, we extend a previous ODE model of gap-junction gating state by Henriquez et al. and formulate it as a system of stochastic differential equations (SDEs) by deriving the expected change vector and covariance matrix of the model and integrating the covariance with respect to a stochastic process, the Wiener Process. In doing so, we construct the first SDE-based model of gap-junction gating dynamics. This SDE description of the electrical coupling between cardiac cells is integrated into a 1D cable model where intracellular current dynamics are described using the Luo-Rudy 1 formulation. Monte Carlo simulations are performed on the resulting model in order to gather data used to construct distributions of several model responses of interest, including conduction block, conduction velocity, gap-junction current and gap-junction conductance. We find a smoothing effect occurs as the number of gap junctions considered increases, but at small numbers of gap junctions, such as those observed in many diseased states, stochastic effects can be pronounced. In such decoupled regimes, stochastic effects are found to have a large effect on the occurrence of conduction block, the cessation of action potential propagation at some tissue location, and are found to increase the variance in conduction velocity from cell to cell. The waiting time between when two consecutive gap junctions reach their maximum current was found to conform to a gamma distribution, with shape and scale parameters a function of the number of gap junctions. As the number of gap junctions increases, the spread of the waiting time distributions decreases. Gap-junctional conductance was modeled as a time-dependent Gaussian distribution, with a temporal variance decreasing as a function of the elapsed time after depolarization. In the case of conduction block, we show that an emulator function can be constructed to estimate the probability of occurrence, thereby reducing the need for a large number of computationally intensive Monte Carlo simulations. Along with probabilistically describing the stochastic gap-junction model, these distributions can be leveraged in larger-scale tissue-level simulations to incorporate stochastic gap-junction gating at a reduced computational cost.

Contents

I. Introduction

Heart disease is the leading cause of death in high-income countries and provides a major strain on global health-care systems [1]. Ventricular fibrillation is one especially deadly form of arrhythmia, which is a collection of conditions defined by irregularity in the heartbeat. Characterized by disordered electrical activity in the heart, ventricular fibrillation is responsible for up to 1 out of every 10 deaths in the United States [1]. There is evidence that the electrical disorganization that characterizes arrhythmia, including ventricular fibrillation, is in part affected by sub cellular processes in cardiac myocytes, the electrically excitable cells constituting the various cardiac tissues [28], [13]. Therefore, it is important to be able to adequately model the electrophysiology of cardiac ventricular myocytes in order to gain a deeper understanding of the relationship between cellular processes and these dangerous conditions.

The cardiac action potential is the sharp increase and subsequent fall of membrane potential in cardiac ventricular myocytes that occurs over roughly 200-300 ms in response to the opening and closing of various voltage-gated ionic channels that line the cell-membrane. Action potentials initiate the contraction process in individual cells, and their propagation from cell to cell allows for the coupled behavior of cells and, on a larger scale, cardiac tissues. This coupling is what ultimately allows for the organized beating of the heart. The voltage upstroke is modulated by these ion channels, which line the membrane of the ventricular myocyte and regulate the flux of ions between the cellular myoplasm and extracellular space. Further, large proteins called gap junctions also line the cell membrane, where they allow for ionic coupling between adjacent cells and assist in the propagation of the action potential [32].

Many of the processes involved in the initiation and propagation of the cardiac action potential at the level of a single cardiac myocyte are reliant on inherently stochastic phenomena [5], [21]. One such example is the voltage-and ionic-concentration-dependent stochastic conformational changes in cellular proteins responsible for the transportation of the ionic species across cardiac cell membranes. Often, the modeling of these stochastic sub-systems is done in a deterministic manner in which it is assumed that the behavior of a large enough collection will have well-defined aggregate properties [28], [13]. Although this approach allows for more computational simplicity than the approach of modeling each stochastic sub-unit individually [10], [26] [22], the deterministic models fail to adequately model the stochasticity present in such a system when the number of coupled subunits is not sufficiently large [31].

In this study, we investigate the applicability of stochastic differential equation modeling to

capture the inherent stochasticity of gap-junctional gating. This approach combines the ability to produce stochastic properties while still tracking population-level dynamics, hence reducing the data storage and processing needs of stochastic models that track the state of each channel individually [26]. We derive a system of stochastic differential equations modeling the population-level gating-dynamics of gap junctions by extending the deterministic ODE model from [11] to the stochastic realm. We then determine several probability distributions on the now-stochastic cardiac processes and discuss ways to integrate the results into other cardiac models [7], as well as compare model distributions with experimental results.

The rest of this thesis is organized as follows: In Section II we give a general overview of the cardiac ventricular action potential and intracellular calcium cycling as well as the electrical coupling between cells via gap junction proteins. In Section III we provide a background into the theoretical formulation of stochastic differential equations as well as a brief overview of the numerical solver used in computing our model. We then derive the system of stochastic differential equations that will model gap-junction gating dynamics and conclude the chapter with model implementation details. In Section IV we use model simulation data to derive probability distributions for several cardiac phenomena of interest. We show that stochastic effects are prominent in poorly coupled cases and that the stochastic system approaches the deterministic system when the number of units becomes arbitrarily large. In Section V we place this research within the wider context of the field by comparing the derived distributions with experimental data and discuss leveraging the distributions to reduce computational demands for tissue-level simulations. We conclude the chapter by introducing preliminary results from a stochastic differential equation model of intracellular Ca^{2+} channel gating. In section VI, we discuss avenues to extend this work and provide several limitations of the current approach.

II. Gap Junction Connectivity

In this chapter we give an introduction to several cardiac processes and how they are necessarily linked in order for the heart to function. The action potential is a central, emergent cardiac process that initializes the contraction process in cardiac tissue and, through cell-to-cell coupling via gap junction proteins, promotes the coordination of this contraction necessary for optimal function. The action potential emerges from changes in intracellular and extracellular ionic concentrations, which are mediated by the gating dynamics of membrane channels that alter their conduction properties in response to local voltage and electrochemical gradients. Upon the membrane-voltage spike that initializes the action potential (depolarization), a large amount of Ca^{2+} is released into the bulk myoplasmic region of the cell, and work is done to subsequently expel or restore the large concentration of free Ca^{2+} in a complicated physiological process known as *calcium cycling*. While in the bulk myoplasmic space, the Ca^{2+} is free to bind to large intracellular proteins (buffers) that initiate the contraction process.

The increase in the intracellular concentration of charged ionic species in a depolarized cell allows for the current pool necessary to travel between adjacent cells via large pore-like proteins lining the cell-membranes, gap junctions, thus initializing depolarization. This general process along with efforts in modeling it are discussed in this section.

II.1 Cardiac Action Potential and Calcium Cycling

The cardiac action potential is a cellular electrophysiological phenomenon characterized by the sharp rise and gradual fall of cell-membrane voltage. The exact form of the action potential varies among the various tissues in the heart. In this paper we will be focusing on the electrophysiology of cardiac ventricular myocytes. In general the ventricular action potential is deconstructed into 5 phases: upstroke (phase 0), early repolarization (phase 1), plateau (phase 2), late repolarization (phase 3) and resting potential (phase 4). Figure 1 shows the voltage form of a typical mammalian action potential from [4]. During phase 0, the resting cell-membrane potential (≈ -80mV) is increased rapidly (to ≈ 30mV) as sodium channels lining the cell membrane open and produce the *fast inward sodium current*. Phase 1 is the result of the activation of the voltage-dependent transient outward potassium current. The plateau phase (2) is marked by a quasi-equilibrium between inward calcium current and several outward potassium currents. Late repolarization (3) is brought about by the initiation of the delayed rectifier potassium currents, which return the cell

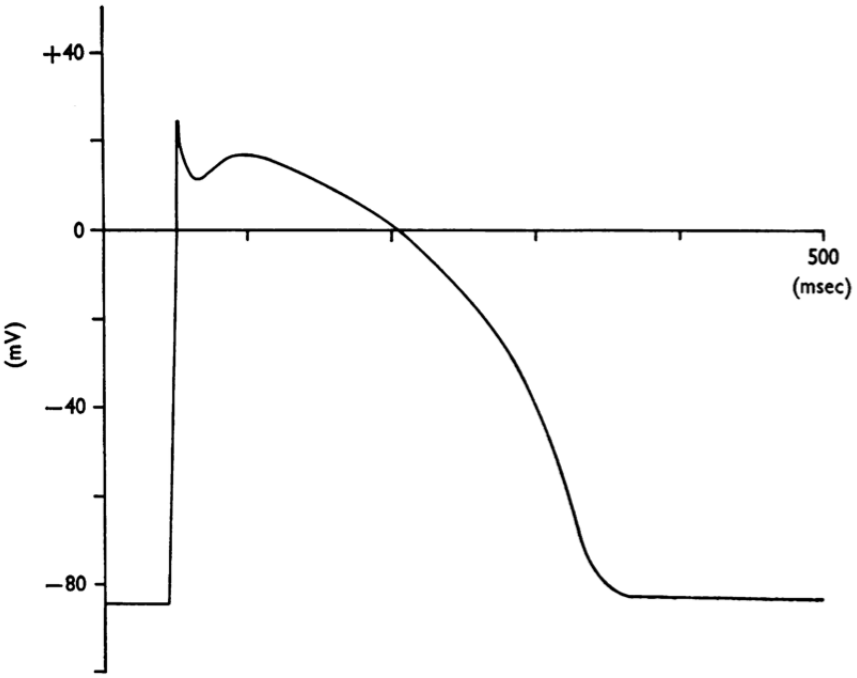

Figure 1: Voltage trace of a typical mammalian action potential from [4]. The fast upstroke corresponds to the rapid depolarization from the fast sodium inward current. The plateau phase is a result of the interplay between inward Ca^{2+} current and outward K^+ current. The slow repolarization phase in which the membrane voltage is returned to the pre-depolarization state is brought upon by delayed K^+ rectifier currents.

to resting membrane potential (4) [32]

Several mechanisms in cardiac cells work against the electrochemical gradient in order to return the ionic concentrations in the cell to their resting values. Two such mechanisms are the Na-Ca exchanger and the Na-K pump, both of which are large proteins embedded in the cell membrane that exchange ionic species between the interior of the cell and the extracellular space [28]. Working in opposition to the sodium gradient, the Na-K pump requires the hydrolysis of ATP in order to export 3 sodium ions for every 2 potassium ions imported, resulting in a net outward current. The Na-Ca exchanger uses the sodium electrical gradient to import 3 sodium ions for every 1 calcium ion exported, resulting in a net inward current, although this can reverse during phase 0 of the action potential in response to the rapid rise in intracellular Na. The activity of the Na-Ca exchanger and Na-K pump contribute to the specific action potential shape [32].

Efforts to model the ventricular action potential have a long history. Ref [20] was a pioneering model of the cardiac action potential, in which the Hodgin-Huxley model of neuronal action

potential initiation and propagation was adapted to model the electrodynamics of a Purkinje cell. The model consists of a set of nonlinear ordinary differential equations that model the conductances of voltage-gated ionic channels, which are used in the computation of the total membrane current of the cell. In 1977, Beeler and Rueter [4] constructed the first model of the ventricular action potential. The model consists of four currents; fast inward Na^+ and slow inward Ca^{2+} currents along with inward and delayed K^+ rectifier currents. In 1991, Luo and Rudy [17] extended the Beeler-Reuter [4] model through the incorporation of two additional currents, the plateau current and an explicit background current, allowing for further refinement of the action potential shape. Four years later, Luo and Rudy extended their original research to incorporate current descriptions for Na-K pump and Na-Ca exchanger along with calcium-induced calcium release (CICR), a process in which a relatively small membrane Ca^{2+} current induces a relatively large release of Ca^{2+} from intracellular stores [18].

More recently, cardiac models have been trending towards increasing physiological detail and complexity. A large investment of modeling has been made to understand CICR. Figure 2 displays a rough schematic representation of the major intracellular currents and structures involved in CICR. CICR is a process in which a relatively small membrane calcium current through L-type channels initializes the opening of ryanodine (RyR) channels, which release a relatively large amount of calcium, stored in a tubular organelle called the sarcoplasmic reticulum (SR) [32]. The calcium that has been released into the cell's bulk cytoplasm is now free to bind to calcium buffers, in particular, troponin, which is influential in initiating the mechanical contraction necessary for the heartbeat [32]. The calcium that does not bind to buffers is actively pumped back into the SR via the sarco/endoplasmic reticulum Ca^{2+}-ATPase (SERCA) pump and into the extracellular space via the Na-Ca exchanger. [10] models CICR via a Markovian description of the gating dynamics of the calcium release unit (CaRU), an aggregate structure comprised of L-type membrane channels and RyR SR channels. The gating state of each CaRU is computed via a Markov chain, which is a function of voltage and local Ca^{2+} concentration. Each gating configuration has a particular associated RyR and L-type current (I_{CaL}) state. The SERCA current is modeled as an ordinary differential equation that is an algebraic function of bulk myoplasmic Ca^{2+} concentration. The model descriptions of RyR, I_{CaL} and SERCA currents are then integrated into the Luo-Rudy II [18] model of ionic currents.

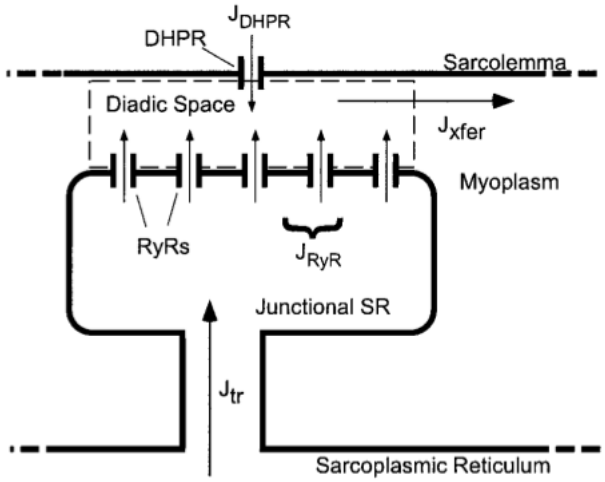

Figure 2: Schematic representation of the major intracellular structures and currents involved in CICR in the venticular myocycte from [25]. Notice the membrane Ca^{2+} flux J_{DHPR} through L-type channels induces the release of SR Ca^{2+} via J_{RyR} flux. RyR and L-type calcium channels can be modeled as a single functional unit, the calcium release unit (CaRU). The bulk cytoplasmic Ca^{2+} from $J_{xfer}$is free to bind to troponin buffers, which initiate contraction.

II.2 Gap-junction Physiology

The direct cell-to-cell communication in most vertebrate animals is accomplished through structures that line the cell membrane called gap junctions. Gap junctions are channel proteins that are composed of two half-channels (referred to as connexons) embedded in the cell membrane of adjacent cells [29] , as shown in Figure 3. Each connexon is composed of six connexins, proteins that are arranged in such a way to form a pore-like structure [8]. The linkage of connexons on adjacent cells to form gap junctions promotes the electrical coupling of cells by allowing an avenue through which charged ions may diffuse between cells.

Gap-junction coupling is thought to be the primary mechanism that allows for the propagation of the cardiac action potential, although recent experiments and modeling efforts [16] have shown that the influence of local electric fields can also have a coupling effect on nearby cells, especially in cases where the number of gap junctions are low due to diseased state. This mode of coupling, known as ephaptic coupling, is an area of active research.

The voltage-induced changes in intracellular ionic concentrations during the onset of an action potential in cell x provide the species available to form the gap-junctional coupling current, I_j,

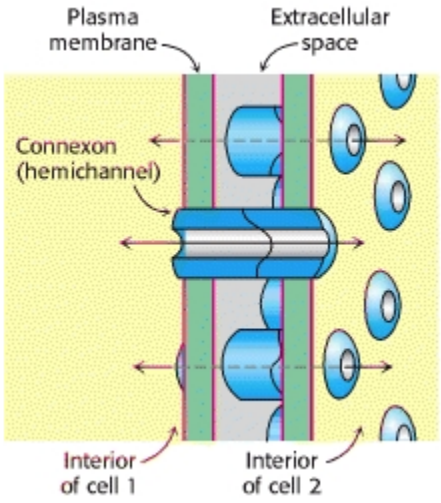

Figure 3: Visual model of cell-to-cell coupling through gap junctions from [5]. Each cell contributes one hemi-channel (connexon) to form a gap junction channel that allows for diffusion of ionic species between cells.

with adjacent cell y. I_j subsequently raises the cell-membrane voltage in cell y to the threshold, which promotes the conformation of sodium channels to the open state, initializing the fast inward sodium current and resulting in the depolarization phase of the action potential [32].

It has been shown that at least two distinct current-producing modes, referred to as the open state and the residual state, exist for each connexon [8]. This conception is a simplification of the actual gating dynamics of gap junctions, as it has been shown that each of the six connexin proteins comprising the connexon serve as sub-gates and a much larger number of distinct gating modes exist [30]. In this context, gating mode refers to the channel's particular conformation among a discrete number of possibilites. The geometry of the channel alters which ionic species are permitted to travel through and as a result its conductive properties. It has also been shown in numerous experiments that the gating dynamics of connexons, and thus gap junctions, are functions of the local gap-junctional voltage gradient [30], [8], [11], [29]. The state of gap junctions is known to follow a Boltzman distribution with respect to gap-junctional voltage. Mouse connexin gating data collected from [30] shows a drop in open probability from $p(O) \approx 0.9$ at 0mV to $p(O) \approx 0.5$ at 37.5mV. Further experiments provide evidence for a chemical dependency in gating configuration, that is, conformation in response to local ionic concentrations, in particular $[Ca^{2+}]_i$ and $[H^+]_i$ [8]. This chemical dependency manifests as a slow, time dependence in inactivation, independent of gap-junctional voltage. That is, $p(O) \to 0$ as $t \to \infty$ at a constant voltage V_0.

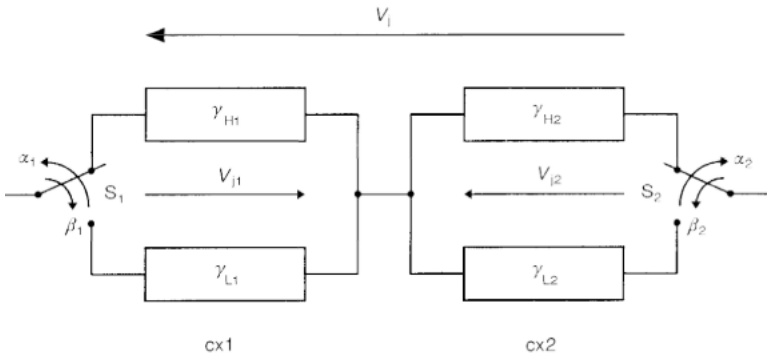

Figure 4: Electrodynamical coupling of two connexons respresented as a circuit diagram from [30]. The circuit senses global gap-junctional voltage V_j and each connexon produces local voltage V_{j1} and V_{j2}. Each connexon has two rate parameters, α and β, governing the switches S_1 and S_2, which re-route current between high (H) and low (L) conductances γ.

Despite the importance of gap junctions in cardiac electrophysiology, relatively few mathematical models have been constructed to describe their gating dynamics, as many cardiac action potential models approximate the behavior with constant intercellular resistance values or smooth out their influence with continuous tissue approximation models [7]. [30] derives a gap junction model describing the dynamics of gap junctions in ventricular myocardium cells. The conductances of each hemi-channel are derived by conceptualizing the two connexons as a series circuit experiencing a constant gap-junctional voltage V_j, represented schematically in Figure 4. The rate parameters of the dynamical system governing gating proportions are modeled as exponentially decaying functions of the local voltage across each connexon. The local gap junction current, I_j, is then computed as the product of the proportion of gap junctions in each of the four gating modes and the associated conductance. The model put forth in [11] aims to describe the propagation of an action potential along a 1D cable model with a voltage-dependent description of gap-junction gating. The model uses the voltage-dependent dynamic gating model from [30] to compute the coupling current I_j and models the intracellular currents using the well known Luo-Rudy I model [17].

The gating dynamics of cellular protein channels are fundamentally a stochastic process. Also, due to the dependence of gap-junction gating dynamics on small changes in ionic concentrations [8], another source of stochasticity in the system results from the stochasticity of molecule position on scales where the notion of concentration breaks down. Several models developed in recent years have attempted to capture this stochasticity in gap junction gating descriptions. [22] and

[21] created 4- and 16-state Markov chains to model the gating dynamics of gap junctions. In computation of the model, the gating state of each gap junction is stochastically simulated from the underlying Markovian description. V_j is then computed as the sum of the voltages across each connexon in the gap junction and the large-scale gating dynamics modeled directly in [30] are emergent properties of the summation of I_j for a large number of stochastically modeled gap junctions.

III. Methods

Stochastic differential equations (SDEs) play an important role in the mathematical modeling of processes that are stochastic (randomly determined) in nature, such as random fluctuations in stock prices, epidemiological disease transmission models, and mechanical vibrations [23], [3], [27]. In this section we present an overview of the theoretical foundation of SDEs, after which we derive a system of SDEs to model the random dynamical nature of gap-junction gating. We must first introduce an important stochastic process, the *Wiener Process*, as it displays the properties that are desired from the stochastic noise we wish to model within the SDE system. Due to the non-differentiability of the Wiener Process, we are forced to refine the traditional definition of the Riemann-Stieltjes integral in order to accommodate the non-smoothness of the solutions to SDEs. Since an SDE defines a stochastic process, the solution to an SDE is but one realization of that process. Hence, we would like not only to compute sample realizations of an SDE, but also to define its high-level probabilistic behavior. We discuss several methods for doing so in this section. After a brief discussion of numerical solution techniques, we conclude the section by deriving the SDE formulation for a model of gap-junction gating dynamics and present implementation details. Intuitively, the stochastic system represents the originally formulated deterministic system along with a component representing white noise. The white noise itself models the stochasticity involved in gating dynamics at the channel level. That is, ion-channel gating is a stochastic process [3].

III.1 Stochastic Differential Equation Formulation

Before presenting the general formulation of a stochastic differential equation we must define several quantities. Let *W(t)* be the continuous-time stochastic process defined for $t \in [0, T]$ satisfying the following properties:

1. $W(0) = 0$.

2. For all s such that $0 \leq s < t \leq T$, the random variable $W(t) - W(s) \sim N(0, \sqrt{t-s})$; that is, $W(t) - W(s)$ is normally distributed with a mean of 0 and a variance equal to the size of the increment.

3. $W(t)$ has independent increments. That is, for $0 \leq u < v < x < y \leq T$, $W(v) - W(u)$ and

$W(y) - W(x)$ are independent random variables.

The stochastic process $W(t)$ satisfying the above three properties is know as the *Wiener Process*, or, more colloquially, *Brownian motion*. The Wiener process is the rigorous mathematical description that captures the random motion of pollen grains suspended in fluid observed in 1827 by botanist Robert Brown [2]. The Wiener process is useful in the formulation of many SDEs since it represents the integral of idealized (white) noise, that is, noise independent of any signal. Hence, it can be used to simulate purely random processes in a model that cannot be handled in a deterministic fashion.

Let $X = [X_1, X_2, ..., X_n]$ be a n-dimensional vector. Then the general form for a stochastic differential equation driven by white noise is as follows:

$$\frac{dX}{dt} = \mu(X, t)dt + \sigma(X, t)dW(t), \tag{III.1}$$

where $dW(t)$ is the derivative of the Wiener process.

Due to the Wiener process being discontinuous almost everywhere [15], (III.1) is actually interpreted as the *integral equation*

$$X(t) = X(0) + \int_0^t \mu(X(s), s)ds + \int_0^t \sigma(X(s), s)dW(s), \tag{III.2}$$

even though it is written in terms of differentials. The first integral is integrated with respect to time and thus the standard formulation of the Riemann-Stieltjes integral can be used for evaluation. The second integral is with respect to a stochastic process and, for reasons discussed in the following sub-section, cannot be evaluated in the same manner as a deterministic integral. In this case we use theory from the Itō calculus, which was developed to extend traditional calculus constructs, such as the integral, to the stochastic domain.

It is also of note that $X(t)$ must necessarily be a continuous-time stochastic process, as its realization at any time t is dependent upon stochastic process *W(t)*.

III.2 Evaluating the Stochastic Integral

To motivate why we must refine our definition of the integral when integrating with respect to a discontinuous stochastic process, such as $W(t)$, let us consider the outcome if we attempt to apply the Riemann-Stieltjes integral in such a situation.

Applying the Riemann-Stieltjes defintion to the second integral in (III.2), we obtain the following;

$$\int_a^b \sigma(X(t),t)dw(t) = lim_{n\to\infty} \sum_{i=0}^{n} \sigma(X(\hat{t}),\hat{t})(w(t_{i+1}) - w(t_i)) \tag{III.3}$$

where $\hat{t} \in [t_i, t_{i+1}]$ and $n = \frac{b-a}{\Delta t}$.

Implicit in this definition is the notion that as $n \to \infty$, $t_{i+1} - t_i = \Delta t \to 0$, and hence $\sigma(X(\hat{t}),\hat{t})$ converges to a consistent value. The issue arises in that $X(\hat{t})$ need not be continuous with respect to t and hence its value depends upon which $\hat{t} \in [t_i, t_{i+1}]$ is taken.

Intuitively, this problem can be solved by fixing $\hat{t}$ within the interval. This is the concept underlying the definition of the Itō integral. The Itō integral is precisely defined as follows:

$$\int_a^b \sigma(X(t),t)dw(t) = lim_{n\to\infty} \sum_{i=0}^{n} \sigma(X(t_i),t_i)(w(t_{i+1}) - w(t_i)); \tag{III.4}$$

that is, we fix that the stochastic function $\sigma(X(t),t)$ is to be evaluated at the left endpoint of each sub-interval $[t_i, t_{i+1}]$, hence making the function evaluation unique.

III.3 Probability Distribution for Stochastic Differential Equations

Let $X(t)$ be a continuous-time stochastic process defined by the stochastic differential equation in (III.1). Evaluating the Itō integral in equation (III.4) will give unique solutions only for unique realizations of the sample path of $W(t)$. Thus (III.4) can be seen as defining a set of sample paths for the stochastic process $X(t)$. With this in mind, a definition of the probability distribution for $X(t)$ can be written to more explicitly characterize its behavior. This is accomplished by solving the *Fokker-Planck-Kolmogorov (FPK) Equation*.

Let $p(X,t)$ be the time-dependent probability distribution for the continuous-time stochastic process $X(t)$. The FPK equation is defined as the following partial differential equation:

$$\frac{\delta p(X,t)}{\delta t} = -\sum_i \frac{\delta}{\delta X_i}(\mu_i(X,t)p(X,t)) + \frac{1}{2}\sum_{i,k} \frac{\delta^2}{\delta X_i \delta X_k}([(X,t)\sigma(X,t)^T]_{ik}p(X,t)). \tag{III.5}$$

The form of the FPK equation does not have as straightforward an intuitive explanation as the formulation of the Itō integral so we will not go into depth regarding its construction. A proof of (III.5) can be found in [2], which relies on computing expectations of arbitrarily-constructed twice-differentiable functions.

Often (III.5) is difficult to solve, yet probabilistic information about the SDE is still desired. In this case, we can attempt to directly compute the time-dependent expectation $m(t)$ and covariance

$V(t)$ of the process $X(t)$ as follows:

$$\frac{\delta m(t)}{\delta t} = E[\mu(X(t), t)], \tag{III.6}$$

$$\frac{\delta V(t)}{\delta t} = E[\mu(X(t), t)(X(t) - m(t))^T] + E[(X(t) - m(t))^T \mu(X(t), t)] + E[\sigma(X(t), t)\sigma(X(t), t)^T]. \tag{III.7}$$

The issue with using (III.6) and (III.7) to circumvent the necessity to compute $p(X, t)$ directly using (III.5) is that the expectation operator is defined by

$$E[\mu(X, t)] = \int \mu(X, t)p(X, t)dX \tag{III.8}$$

and thus requires knowledge of $p(X, t)$ to compute. That being stated, we can assume a Gaussian $p(X, t)$ and use (III.6) and (III.7) to form a Gaussian approximation of the moments.

Another option to derive the probability distribution for (III.1) is to use Monte Carlo simulation methods. That is, we can compute a large number of sample paths using an SDE numerical solver (covered in the following section) and fit a parametric probability distribution to the resulting data. This approach will be covered later in this thesis as the method chosen for approximating the probability distributions of various gap-junction model responses is discussed.

III.4 Numerical Solvers

Here we give a brief overview of one common numerical solution technique for stochastic differential equations of the form (III.1). We compute the solution over the interval $[0, T]$ and we define $\Delta t = \frac{T}{N}$ and $t_i = i\Delta t$, for $i = 0, 1, ..., N$.

The *Euler-Maruyama method* is the extension of the Euler method to stochastic differential equations. Applying the method to the general form of (III.1) gives

$$X_i = X_{i-1} + \mu(X_{i-1}, t_{i-1})\Delta t + \sigma(X_{i-1}, t_{i-1})(W(t_i) - W(t_{i-1})), \tag{III.9}$$

where $W(t)$ is the the realization of the Weiner process at t.

The systems of SDEs in this paper were solved using an implementation of the Euler-Maruyama method. Although used widely, this method suffers from some of the same problems as its deterministic counterpart, e.g., a slow rate of convergence as $\Delta t \to 0$. Analogous to numerical ODE and PDE solvers, there exists a whole family of solution methods derived from the Taylor series expansion of the SDE. For more information on alternate solvers, see [27].

III.5 Model Framework: Stochastic Gap Junction

We now consider the derivation of a novel stochastic differential equation model from the deterministic gap-junction gating formulation in [11]. Although the model in [22] incorporates the stochasticity of gap-junction gating dynamics, the computation of the model relies on the simulation of the gating state of M gap junctions coupling adjacent cells. In the 1D cable model computed in [11], $N = 300$ cells, each being coupled to its neighboring cells by anywhere from $M = 80$ to $M = 6,700$ gap junctions, were simulated. These types of simulations would quickly become computationally expensive if $N\dot{M}$ gap-junction states were required to be computed individually every time step. By approximating the population-level effects of the stochastic gating of individual gap junctions using an SDE model, we are able to reduce the computational strain in data storage and processing involved in stochastically simulating each gap junction's gating state while recovering the inherent stochastic noise of the phenomenon not considered in the ODE formulation.

In this study, propagation of an action potential was modeled on a one-dimensional fiber consisting of 300 cardiac cells. The model consists of a description of the membrane currents for each individual cell along with a component describing the voltage-dependent gap-junction coupling between cells. The membrane current of each cell was described using the Luo-Rudy I model [17]. This model provides a phenomenological description of the major transmembrane currents. The gap-junction coupling is described by the current $I_{junc}(t)$, which is itself a function of the proportion of coupled gap-junction channel proteins in one of four defined conformational states, $X = [HH, HL, LH, LL]$. Hence, for adjacent cells i and $i+1$, state YZ refers to the conducting state of a connexon on cell i being in state Y and the corresponding connexon on cell $i+1$ in state Z. The conducting states can be in either the high state H or the low state L. The conductances of each of the four aggregate states are derived using basic principles of circuit theory. The gap-junction conformation rates are described using exponential functions of the voltage across each configuration whose parameter values have been estimated experimentally [30].

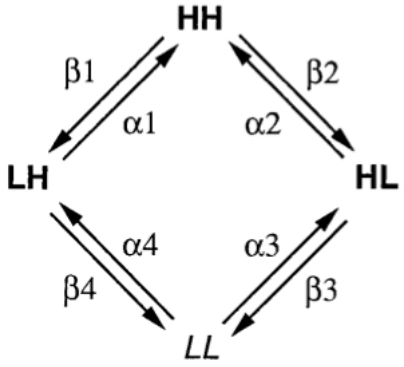

Figure 5: Dynamic gap-junction gating schematic from [11]. States $\{HH, HL, LH, LL\}$ refer to the pairing of distinct gating configurations, H for high-conducting mode and L for low-conducting model. Parameters $\{\alpha_1, \alpha_2, \alpha_3, \alpha_4, \beta_1, \beta_2, \beta_3, \beta_4\}$ are rate parameters that govern transitions between the aggregate gating modes. Parameter values have been estimated experimentally and can be found in [11].

The model consists of gating states X along with the set of rate parameters: $\{\alpha_1, \alpha_2, \alpha_3, \alpha_4, \beta_1, \beta_2, \beta_3, \beta_4\}$ and a system of ODEs describing model transitions:

$$\frac{dx_1}{dt} = -(\beta_1 + \beta_2)x_1 + \alpha_1 x_2 + \alpha_2 x_3,$$

$$\frac{dx_2}{dt} = -(\alpha_1 + \beta_4)x_2 + \beta_1 x_1 + \alpha_4 x_4,$$

$$\frac{dx_3}{dt} = -(\alpha_2 + \beta_3)x_3 +_2 x_1 + \alpha_3 x_4,$$

$$\frac{dx_4}{dt} = -(\alpha_3 + \alpha_4)x_4 + \beta_4 x_2 + \beta_3 x_3,$$

where

$$\{x_1, x_2, x_3, x_4\} = \{n(HH), n(HL), n(LH), n(LL)\} \quad \text{(III.10)}$$

and $n(x)$ is the proportion of gap junctions in the x_i configuration.

Transition	*Probability*
$\Delta X^1 = (-1, 1, 0, 0)^T$	$\beta_2 x_1 \Delta t$
$\Delta X^2 = (1, -1, 0, 0)^T$	$\alpha_2 x_2 \Delta t$
$\Delta X^3 = (0, -1, 0, 1)^T$	$\beta_3 x_2 \Delta t$
$\Delta X^4 = (0, 1, 0, -1)^T$	$\alpha_3 x_4 \Delta t$
$\Delta X^5 = (0, 0, -1, 1)^T$	$\beta_4 x_3 \Delta t$
$\Delta X^6 = (0, 0, 1, -1)^T$	$\alpha_4 x_4 \Delta t$
$\Delta X^7 = (-1, 0, 1, 0)^T$	$\beta_1 x_1 \Delta t$
$\Delta X^8 = (1, 0, -1, 0)^T$	$\alpha_1 x_3 \Delta t$

Table 1: Possible transitions in the discretely formulated gap-junction gating model along with associated probabilities. Transitions are defined to be occurring over a sufficiently small interval Δt in which it can be assumed that the probability of more than one transition is of measure 0. The existence of such an interval is guaranteed if we assume the transitions are governed by a Poisson process.

Consider a discrete analog of the above system; that is, instead of modeling the dynamics of the proportion of gap junctions in a given gating mode, we model the *number* of gap junctions in a given gating mode. In order to derive a stochastic extension of the above system, we study its behavior over a *sufficiently small* time step Δt. If the transition of a single gap junction from state x_i to x_k is assumed to follow a Poisson distribution, as is the standard in compartmental models [6], we can then assume that as $\Delta t \to 0$, the probability of more than one gap junction transitioning states in time interval Δt also goes to 0. Let $\Delta X^i = (\Delta x_1, \Delta x_2, \Delta x_3, \Delta x_4)^T$ represent the i^{th} possible discrete change in the system. Table 1 defines each such possible transition and associated probability.

We are then able to define the expected change vector and covariance matrix of the discrete stochastic system as follows:

$$E(\Delta X) = \sum_{i=1}^{n} \Delta X^i p_i$$

$$E(\Delta X (\Delta X)^T) = \sum_{i=1}^{n} p_i \Delta X^i (\Delta X^i)^T.$$

(III.11)

Note that from this definition the expected change vector is the weighted average of all possible transitions the system can make. The covariance matrix is a representation of how any two states change together. It is a symmetric matrix by definition, since the ij^{th} and ji^{th} entries both describe how states i and j change together (co-vary).

We can approximate the continuous-time analogs to the quantities defined in III.5 in the following manner:

$$\mu(\vec{X},t) = \frac{E(\Delta X)}{\Delta t},$$

$$V(\vec{X},t) = \frac{E(\Delta X(\Delta X)^T)}{\Delta t}\ .$$

(III.12)

The continuous-time approximations in III.5 can be thought of as a type of limiting process; as we choose smaller Δt intervals, the expected distance between the continuous and discrete systems approaches 0. That is,

$$lim_{\Delta t\to 0} E(|\frac{E(\Delta X)}{\Delta t} - \mu(\vec{X},t)|^2) = 0$$

and

$$lim_{\Delta t\to 0} E(|\frac{E(\Delta X(\Delta X)^T))}{\Delta t} - V(\vec{X},t)|^2) = 0$$

(see ref [2]). Further, it can be shown that V is not only symmetric but positive semi-definite, i.e., $x^T V x \geq 0, \forall x \in \mathbb{R}$, from which it directly follows that there exists some B such that $B^2 = V$ and B is unique, (see ref [2]).

We may now define the stochastic gap-junction gating model as follows;

$$X_{t+s} - X_t = \int_t^{t+s} \mu(X,t)dt + \int_t^{t+s} B(X,t)dW. \tag{III.13}$$

where $W(t)$ is a four-dimensional Wiener process and the second integral in III.3 is defined by the Itō calculus. Alternatively, we may write III.13 in conventional differential notation,

$$dX_t = \mu(X_t,t)dt + B(X_t,t)dW_t. \tag{III.14}$$

.

III.6 Implementation Details

The stochastic gap-junction model is integrated into a 1D cable model in which the intracellular current dynamics for each computational node are described by the Luo-Rudy I current model. Instead of a diffusive description, as is standard in 1D cable model formulations [7], the coupling current between nodes in gating configuration x and y is modeled by the stochastic gap-junction gating model derived in the previous section. This is accomplished by using the Matlab function *fsolve*, which uses an implementation of Newton's method to solve the following implicitly defined system of equations for each gap-junction unit:

$$V_{jx} = -V_j(\frac{g_y}{g_x+g_y})$$

$$V_{jy} = V_j(\frac{g_x}{g_x+g_y}),$$

(III.15)

where

$$g_x = \Lambda_x e^{\frac{-V_j x}{V_x}}$$

$$g_{xy} = \frac{g_x g_y}{g_x+g_y},$$

(III.16)

with V_j the local gap-junction voltage, g_{xy} the conductance across the gap junction connecting nodes in gating state x and y, V_{jx} the half-channel voltage and Λ_x the constant maximum conductance of a half-channel in state x.

The coupling current is then computed as

$$I_{junc}(t) = N < X, G > V_j(t), \tag{III.17}$$

where N is the number of gap junctions, $X = [x_1, x_2, x_3 x_4]$, and $G = [g_{HH}, g_{HL}, g_{LH}, g_{LL}]$.

Due to the heavy computational expenses of this simulation, efforts were made to vectorize the computation of the covariance matrices and expectation vectors. We define data structures

$$C_t = \begin{vmatrix} c_{11} & c_{12} & c_{13} & c_{14} \\ c_{21} & c_{22} & c_{23} & c_{24} \\ c_{31} & c_{32} & c_{33} & c_{34} \\ c_{41} & c_{42} & c_{43} & c_{44} \end{vmatrix}$$

and

$$E_t = \begin{vmatrix} e_{11} & e_{21} & e_{31} & e_{41} \end{vmatrix},$$

where c_{ij} is the m-dimensional vector holding the ij^{th} element of the square root of the covariance matrix for all m computational nodes and e_{i1} is the m-dimensional vector holding the i^{th} element of the expectation vector, both at time step t.

Letting

$$W = \begin{vmatrix} W_1 \\ W_2 \\ W_3 \\ W_4 \end{vmatrix},$$

where each W_i is an m-dimensional vector of a single Wiener-process realization, the stochastic gap-junction model can be computed efficiently at each time step in the following manner:

$$\Delta X_t = E_t dt + C_t W, \tag{III.18}$$

where

$$\Delta X_t = \begin{vmatrix} \Delta x_1 \\ \Delta x_2 \\ \Delta x_3 \\ \Delta x_4 \end{vmatrix}$$

holds data describing the change in gap junction gating proportions for all four configurations, for each node m. This process of vectorizing the data lends to efficient computation in Matlab by allowing the use of built-in vector and matrix operations.

All simulations were run with parameter values describing intracellular current dynamics given by the Luo-Rudy 1 model. A cable of $m = 300$ computational nodes was used in all simulations and a time step of $\Delta t = 0.01$ms was used in the integration of the model, accomplished with the

forward Euler method. The stochastic gap-junction model was simulated using an implementation of the Euler-Maruyama method. Parameter values for the gap-junction model were taken to be those supplied in the original deterministic formulation.

IV. Results: Stochastic Gap Junction Connectivity

Gap-junction connectivity allows direct electrical coupling between adjacent cardiac cells and promotes the propagation of action potentials through cardiac tissue. It has been shown that gap junctions change conformation, and as a result conductive properties, as a function of local voltage [11]. Further, it has been shown that the conformational changes in such proteins are stochastic in nature [21]. Here, we formulate a novel approach to modeling gap-junction gating behavior by introducing a stochastic differential equation-based description for the proportion of gap junctions in one of four gating states. This description of cell-to-cell coupling is integrated into a 1D cable model, where the intracellular current dynamics for each cell are computed using the Luo-Rudy 1 model [17]. Since our model is stochastic in nature, we would like to obtain a probabilistic description of several phenomena of interest as well as analyze the effects that varying numbers of gap junctions have on the characteristics of these distributions. We begin the analysis of our model by investigating stochastic effects on conduction block, where we devise a binomial experiment to probabilistically evaluate the likelihood of conduction block in the poorly coupled (small number of gap junctions) case. Next, we assess the effect of stochastic gating on the conduction velocity of the action potential by computing the speed at which action potentials propagate from cell to cell, again in the poorly coupled case. We then derive probability distributions modeling the elapsed time between the maximum value (in magnitude) of the gap-junctional current of two adjacent gap junctions as well as the gap-junctional conductance as a function of time after depolarization.

IV.1 Conduction Block

We begin the analysis of our model by investigating stochastic effects on conduction block, which is a tissue-level phenomenon in which an action potential's propagation is halted or blocked. Conduction block is known to occur in tissue that, due to genetic reasons or a diseased state, is poorly coupled on the cellular level, that is, the number of gap junctions electrically coupling the cell is reduced dramatically [14]. Because of the small number of gap junctions, the stochastic effects are most pronounced in the poorly coupled case, so we hypothesize that the stochasticity in our model will be influential in regimes that allow conduction block to occur.

We begin by determining the number of gap junctions, N, in which conduction block begins to occur. To accomplish this, we use a bisection algorithm over the range $N \in \{50, 51, ..., 90\}$, as

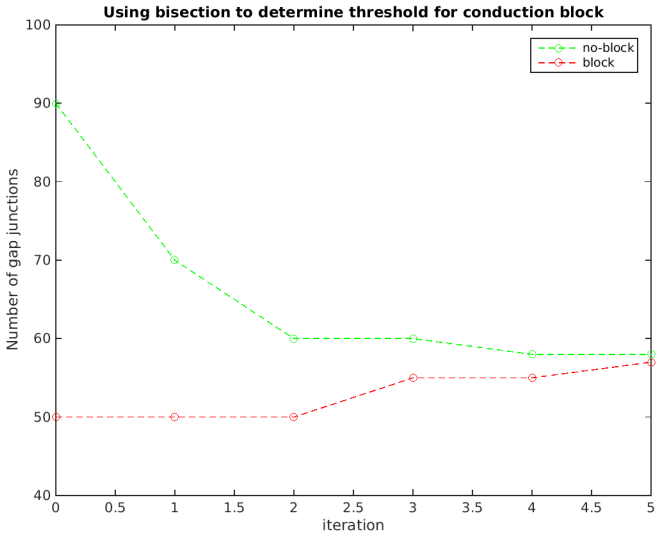

Figure 6: Convergence diagram for the bisection method used in determining the threshold number of gap junctions to induce conduction block in the deterministic gap-junction model. We investigate the range $N \in \{50, 51, ..., 90\}$ in accordance with the what has been reported in literature and find that block occurs between 57 and 58 gap junctions.

this is the region in which block begins to occur in [11]. We assess if the given number induces conduction block by using a method that searches the spatio-temporal voltage data to determine if and where block occurs. Note that the stochastic component of the differential-equation model describing gap-junction dynamics was removed temporarily while performing this search to ensure that the resulting block-inducing number is independent of any stochastic fluctuations specific to a given trial. The threshold for conduction block is found to occur between 57 and 58 gap junctions, where 58 gap junctions is the lower bound that allows propagation through the entire cable. The convergence traces for the bisection method are displayed in figure 6.

Having determined the threshold number of gap junctions for inducing block, we now implement the stochastic description of gap-junction gating dynamics and study the effect on conduction block near this threshold. To obtain a probabilistic description of conduction block, we construct a binomial experiment in which for each trial an action potential is initialized at one end of the cable and its propagation is studied. A success is defined as the simulation exhibiting no conduction block, while a conduction block at any position in the cable is a failure. Data was gathered from a total of 25 simulations run for each of several values of N in a range close to where block occurs. The results of the experiment are displayed in Table 2. As the number of gap junctions increases

Number of Gap Junctions	*Block*	*No Block*	$\hat{p}$
52	25	0	0.0
54	24	1	0.04
56	20	5	0.20
57	20	6	0.24
58	11	14	0.44
60	2	23	0.92
70	0	25	1.0

Table 2: Results of binomial experiments for several different numbers of gap junctions. Notice that as the number of gap junctions is increased, the probability of conduction block becomes negligible.

the binomial success parameter p tends towards 1, while as N decreases p tends toward 0. This positive relationship is expected, as with increasing values of N over the threshold for conduction block in the deterministic formulation, it becomes increasingly less likely that random stochastic fluctuations will block propagation.

To validate the probabilistic behavior of the stochastic gap-junction model's predictions on conduction block, we compare them to those of the deterministic formulation. Recall that the deterministic formulation of the model predicts conduction block to onset at $N = 57$ gap junctions. Further, we expect the stochastic model to fluctuate around the deterministic one, since the source of randomness is modeled as Gaussian white noise. In other words, the probabilistic behavior of the stochastic gap-junction model should have well defined average properties that actually recover the predictions of the deterministic system.

We begin by making a normal approximation to the binomial distribution of conduction block data, as shown in Figure 7. For a fixed number of gap junctions, conduction block *not* occurring in the deterministic model is analogous to the proportion of trials in our binomial experiment that result in a *success* being larger than 0.5 in the stochastic model, as the number of trials becomes arbitrarily large. This is because the average properties of the stochastic system should define the deterministic one; thus, $p > 0.5$ is equivalent to no block or $p = 1$ in the binary deterministic setting. We test the hypothesis that the binomial experiment data collected for $N = 57$ and for $N = 58$ come from a distribution with $p > 0.5$. The results are summarized in Table 3.

The p-value measures the probability for obtaining a statistic as extreme or more extreme than the one obtained from a given hypothesized distribution. At a significance level of 0.05, the p-value

Number of Gap Junctions		*p-value for* $H_0 : p < 0.5$
57	0.24	$4.94x10^{-4}$
58	0.44	0.2756

Table 3: Testing the fit of the binomial data to a distribution with $p > 0.5$, which would indicate no conduction block in a binary system. The p-value for the experiment with $N = 57$ indicates that the default binary behavior of the system promotes conduction block, which is in agreement with our findings in analyzing the deterministic system.

for the case of 57 gap junctions indicates that it is highly unlikely that the data came from an underlying distribution with $p > 0.5$, as $4.94x10^{-4} \ll 0.05$. For the case of 58 gap junctions, the p-value is computed to be 0.2756, which indicates that the hypothesis that the data results from an underlying distribution with $p > 0.5$ is valid at any reasonable significance level.

We can also approximate the functional relationship between the binomial probability of success and the number of gap junctions in a given simulation. In order to promote convergence in the fitting algorithm, the number of gap-junctions was normalized to fall between 0 and 1 using IV.1, where $N_{max} = 70$ and $N_{min} = 52$, the maximum and minimum number of gap junctions considered in our simulations.

$$N\prime = \frac{N - N_{min}}{N_{max} - N_{min}} \tag{IV.1}$$

$$p_N \approx \frac{1}{1 + ae^{-bN}} \tag{IV.2}$$

A logistic dependence between the binomial success parameter and the number of gap-junctions was postulated (IV.2) and curve-fitting functionality in Matlab was used to determine the function parameter values a and b that minimized the residual. The Levenberg-Marquardt algorithm was implemented to solve the nonlinear optimization problem. The optimized parameter values were found to be $a = 327.8$ and $b = 17.7$, giving the model an $r^2 = 0.9876$ fit to the simulation data. Figure 8 shows a plot of the data and logistic functional fit over the normalized number of gap junctions investigated. The high r^2 value indicates a strong fit of the model to the binomial data.

The derived logistic functional relationship between the number of gap junctions N and the binomial success parameter p can now be used as a type of statistical emulator. That is, if we desire to estimate p for any number of gap junctions between 52 and 70, we need not run the computationally expensive Monte Carlo simulation of our model to obtain the data necessary

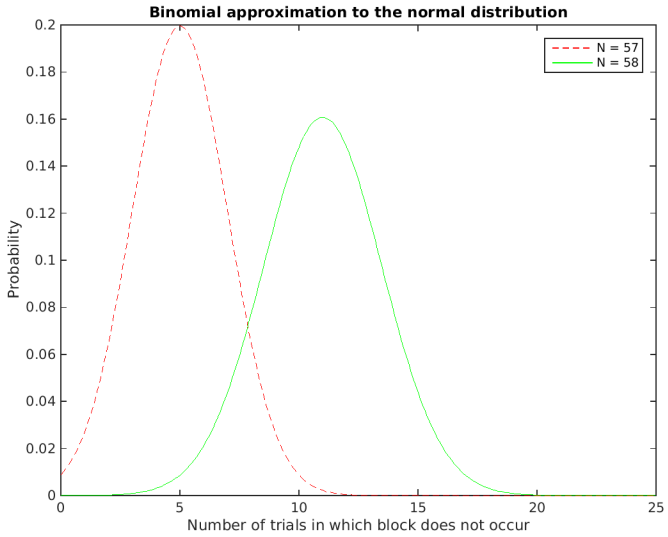

Figure 7: Normal approximations of the binomial data gathered for stochastic conduction block trials. The spread of the curves indicate the data for $N = 57$ gap junctions is from a distribution whose average behavior would promote conduction block, in accordance with expectations based on the deterministic model.

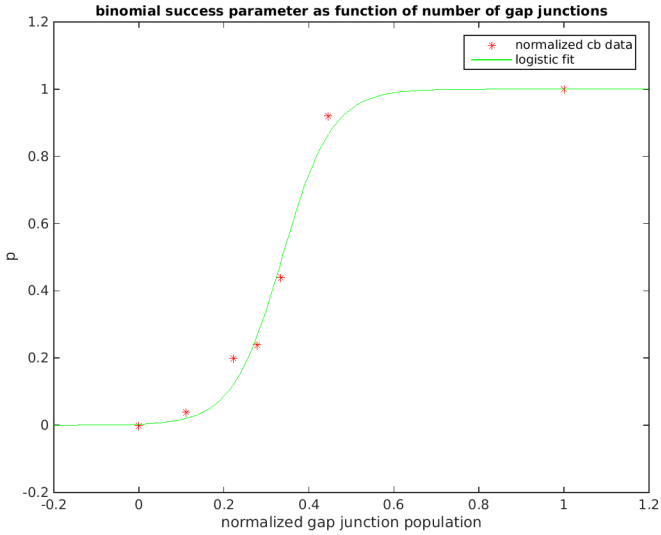

Figure 8: Plot of the binomial success probability as a function of the normalized number of gap junctions along with the logistic model of the dependence.

for direct estimation. Instead, we can leverage the logistic function to provide an inexpensive prediction for p needing only the parameters a and b as well as the desired number of gap junctions N.

IV.2 Conduction Velocity in the Poorly Coupled Case

Gap junctions provide the channels that electrically couple cardiac cells. The strength of this electrical coupling directly influences the speed at which the action potential propagates through tissue, referred to as the conduction velocity. When analyzing conduction velocity in which the gap-junction gating proportion is modeled as a stochastic process, the speed of propagation is also a stochastic process with realizations at each computational node (cell) in the cable. Thus, to characterize the conduction velocity, we must obtain a probabilistic description of this process.

Let $\{V_i^N\}_{i=1}^M$ be the stochastic process describing the conduction velocity on a 1D cable of M cells each coupled by N gap junctions. Note that due to the structure of the model, the only coupling between cells is through gap junctions connecting adjacent cells. Thus we can assume no auto-correlation in the process; that is,

$$cov(V_k^N, V_j^N) \approx 0 \text{ for } k \neq j \tag{IV.3}$$

Further, the source of stochasticity in the model is Gaussian white noise, which is normally distributed with a mean of zero. This implies that the stochastic fluctuations in model states will be about the predictions of the original deterministic formulation, which allows only constant cell-to-cell conduction velocity. Together with the homogeneity in the distribution of the number of gap junctions (each cell-to-cell coupling is through a constant N gap junctions) this allows us to conclude that $\{V_i^N\}_{i=1}^M$ must be a stationary process with respect to both space and time; that is,

(IV.4)

$$E[V_k^N] = E[V_j^N]$$

$$Var[V_k^N] = Var[V_j^N]$$

$$\text{for all } j, k \in [1, 2, ..., m].$$

From IV.3 and IV.4, we have shown $\{V_i^N\}_{i=1}^M$ to be a stationary process. We are now able to use theory developed for such processes in order to characterize its distribution. In particular, we are

able to produce an unbiased estimation of the mean and variance of the process directly from the mean and variance of the sample realizations.

A Monte Carlo method is used to generate sets of process realizations for several values of N near the threshold for conduction block, determined experimentally through the bisection scheme presented in the previous section. In each simulation, the model is run for 1000ms with a time step $\Delta t = 0.01$ms. The cable is comprised of $M = 300$ computational nodes (cells) and each cell-to-cell junction has an instance of the stochastic gap-junction model describing coupling dynamics computed in parallel to increase computational speed. The intercellular distance was taken to be a constant 100μm, in accordance with the value used in [11]. An implementation of the forward Euler method was used to integrate the cable model with an Euler-Maruyama scheme used to solve the stochastic gap-junction model. The voltage is supplied to the cable by instantiating the voltage of the first cell to -30mV. The parameter values used in the Luo-Rudy I description of cellular currents are taken to be the same as [17].

Compiling the results of our simulation, Table 4 displays the average mean and standard deviation for a sample of 25 process realizations for several different numbers of gap junctions. We find that increasing the number of gap junctions per cell increases the mean conduction speed while reducing the variance of the process. Figure 9 shows a single process realization over several values of N. As N increases, there is an evident smoothing in the magnitude of stochastic fluctuations as well as an upward trend in where the process realizations reside. This information is more easily discernible in Figure 10, which shows a clear positive linear relationship between the average conduction velocity and the number of gap junctions. Further, the variance of the process as a function of the number of gap junctions suggests an exponential decay relationship.

As stated, the mean of the stochastic process $\{V_i^N\}_{i=1}^M$ should recover the conduction velocity of the deterministic formulation. Therefore, the positive relationship between mean conduction velocity and the number of gap junctions is in agreement with the positive relationship between conduction velocity and the number of gap junctions in Ref. [11]. The decay relationship between the standard deviation of the conduction velocity and the number of gap junctions indicates a smoothing in stochastic fluctuations as increasing numbers are considered. This result is consistent with the smoothing observed in the calcium current at increasing numbers of CaRUs in the stochastic CaRU gating model [31]. Although the stochastic gap junction and stochastic CaRU models have different cellular gating proteins, the fundamental smoothing tendencies are identical.

Number of Gap Junctions Per Cell	Mean (cm s^{-1})	*Standard Deviation* (cm s^{-1})
58	$47.67 * 10^{-3}$	$12.65 * 10^{-3}$
60	$52.23 * 10^{-3}$	$9.12 * *10^{-3}$
70	$64.55 * 10^{-3}$	$5.2 * 10^{-3}$
80	$77.33 * 10^{-3}$	$4.60 * 10^{-3}$

Table 4: The aggregate mean and standard deviation values for the conduction velocity in the stochastic gap-junction model. The mean conduction velocity increases and the standard deviation of the process decreases with increasing values of N. The inverse relationship between N and the standard deviation is the result of smoothing effects from many coupled stochastic units.

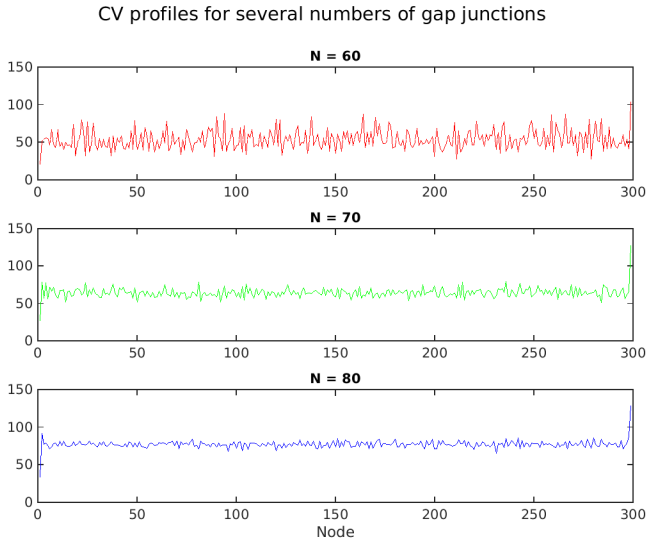

Figure 9: Process realizations for several values of N. The magnitude of stochastic fluctuations tends to decrease for increasing values of N while the mean of the process increases.

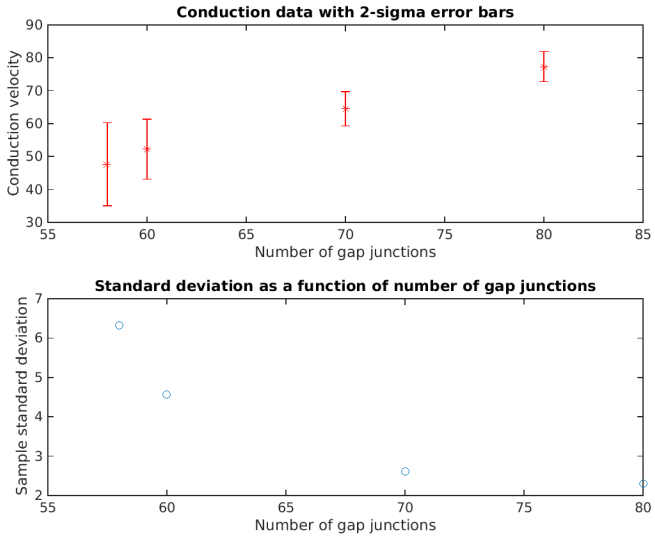

Figure 10: Aggregate mean and 2-sigma error bars for the conduction velocity for several values of N. The mean speed of conduction increases with increasing N while the standard deviation of the process decays in an exponential-like manner. In other words, the process approaches the deterministic approximation as $N \to \infty$.

IV.3 Probabilistic Description of Gap-junction Current

Along with ephaptic coupling, the gap-junctional current is one of the two most important modes of coupling between cardiac cells [19]. Without it, the propagation of action potentials among cells, and as a result coordinated contraction, would be more difficult to achieve. The two previous sections showed that the stochastic description of gap-junction gating dynamics resulted in the necessity for conduction block to be described probabilistically as well as for conduction velocity to be modeled as a stochastic process. Both of these phenomena are fundamentally high-level results of the stochastic nature of the gap-junction current. In particular, if we define the collection $\{A_i^N\}_{i=1}^M$, where A_i^N is the random variable representing the time between gap junctions i and $i+1$ reaching their maximum (in magnitude) current values for a regime with N gap junctions and M cells, then both conduction block and conduction velocity are intimately related to this process.

Due to the independence of gap-junction dynamics, we can assume each A_i^N is governed by the same probability distribution for a fixed N. Thus, $\{A_i^N\}_{i=1}^M$ is fundamentally a process modeling the waiting time between two stochastic events, in our case, the time in which two consecutive gap

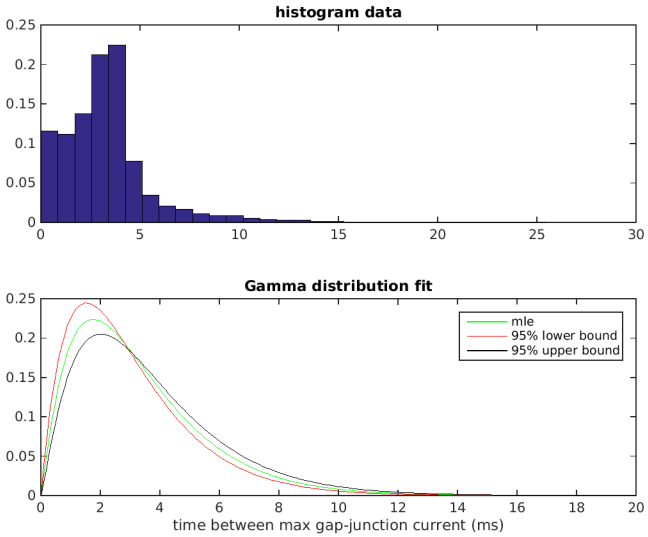

Figure 11: (Top panel) Frequency histogram of waiting-time data collected from the subset of simulations that experienced no conduction block for $N = 58$ gap junctions. (Bottom panel) The gamma pdf curves constructed by the maximum likelihood estimate, 95 % upper and lower bounds for shape and scale parameters k and θ.

junctions produce their maximum current. In operations research and econometrics applications, the probability distributions of waiting times are often modeled using a gamma-distribution, with shape parameter k and scale parameter θ. We begin by modeling the waiting-time distribution for the case of $N = 58$ gap junctions. To conduct analysis, we collect simulation data from our model with $N = 58$ gap junctions. We discard data from trials in which conduction block occurred, as waiting times for nodes after block would be meaningless. The Monte Carlo simulation was run until data were collected from 25 trials in which no conduction block occurred.

Figure 11 (top panel) shows a frequency histogram of the waiting time data collected from simulations. Matlab functionality was used in order to determine the maximum likelihood estimates for the gamma distribution shape and scale parameters k and θ, displayed in Table 5 along with the first two moments of the distribution. The resulting gamma pdf curves for all 3 parameter combinations are plotted in Figure 11 (bottom panel). The strong positive skew of the data indicates that wait times to the right of the median have larger spread than those to the left of the median. The right tail can be interpreted as stochastic fluctuations, that is, trials in which wait times were blocked by stochastic reductions of the proportion of gap junctions in the high-conducting (HH) gating mode. Thus we expect a reduction in the skew of the data as the

	k	θ	$\mu = k\theta$ (ms)	$\sigma^2 = k\theta^2$ (ms)
MLE	2.13	1.56	3.32	5.18
95 % upper bounds	2.03	1.48	3.00	4.45
95 % lower bounds	2.23	1.64	3.66	6.00

Table 5: Maximum likelihood estimates (MLE) along with 95 % confidence upper and lower bounds for gamma-distribution shape and scale parameters k and θ modeling waiting-time data collected from simulations with $N = 58$ gap junctions. The mean μ and variance σ^2 computed as functions of gamma shape and scale parameters.

number of gap junctions is increased and stochastic fluctuations are smoothed out.

Akin to analysis on conduction block and velocity, it would be useful to get a sense of how the probabilistic behavior of waiting-time distributions changes with respect to the number of gap junctions under consideration. We have seen that the stochastic behavior of our model is most pronounced when the number of gap junctions is small, that is, in the poorly coupled regime. The distribution of waiting times is no different.

In Figure 12, we plot the gamma pdf generated from the maximum likelihood estimates for shape and scale parameters k and θ based on data gathered for several numbers of gap junctions. Notice the spread of the distribution decreases inversely with respect to N, although the time at which the pdf reaches its maximum, t_{max}, is approximately constant at $\approx$ 2ms. As the number of gap junctions increases, the current has more avenues to propagate between cells and hence the long waiting times, realized in the pdf as the strong right skew, become increasingly rare events.

Table 6 compiles the shape/rate parameters, first two moments and t_{max} for several values of N around conduction block. There is a decrease in both the mean and the variance of the distribution as N increases while t_{max} holds relatively constant.

N	k	θ	μ	σ^2	*time of maximization (ms)*
54	1.63	2.58	4.21	10.85	1.87
57	1.70	2.22	3.77	8.38	1.93
58	2.13	1.56	3.32	5.18	1.91
60	5.62	0.40	2.25	0.90	2.01

Table 6: Maximum likelihood estimates (MLE) for gamma-distribution shape and rate parameters k and θ along with the first two moments and the waiting time that maximizes the distribution. Although the pdfs vary in shape, all are maximized at ≈ 2 ms, the waiting time in the deterministic formulation of the model.

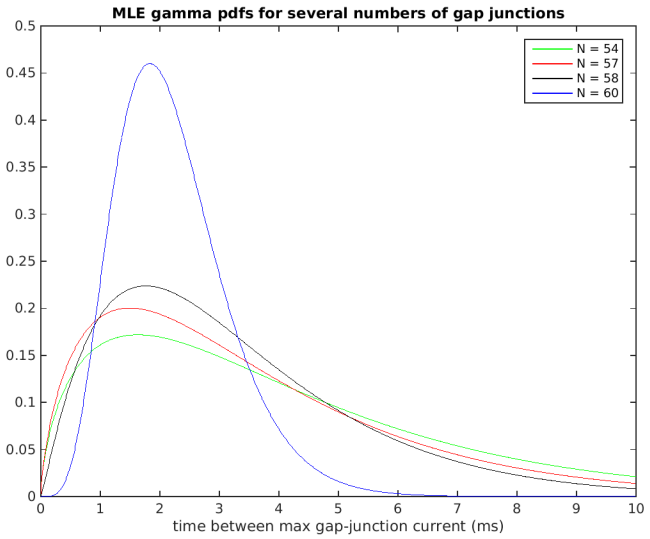

Figure 12: The maximum likelihood gamma distribution fits for $N = 54, 57, 58$ and 60 gap junctions. The spread of the pdf decreases as N increases. Further, all curves reach their maximum at ≈ 2ms, the waiting-time in the deterministic model.

IV.4 Probabilistic Description of Gap-junction Conductance

Conductance is a measure of the ease with which electrical current is able to pass, that is, the inverse of electrical resistance. Due to the stochastic voltage-induced inhibited gating in our model, the depolarization of cell i will induce a stochastic transient decrease in conductance in the gap junction connecting cell i to cell $i+1$. A probabilistic description of this transient fall and subsequent rise in gap junction conductance is desired as a function of the time elapsed after depolarization of the previous cell.

Although there is no method that is universally accepted for detecting the instant of depolarization, various voltage threshold and slope criteria are used for this purpose. In this study, we will use a threshold of $-40mV$ as the marker for depolarization. That is, we use the time at which a cell's voltage, previously at resting potential, climbs above -40mV as the time of depolarization (t_0). We then collect the gap-junction conductance data until it rises back near the conductance at resting potential. Figure 13 shows several time series profiles for post-depolarization conductance data gathered at a particular node in the middle of the cable over separate simulations, all with a constant number of $N = 60$ gap junctions. The conductance plateau period realized in the top and middle conductance profiles is not present in the bottom conductance profile. This is an indication that the channel gating stochasticity is not simply inducing noise around a well defined mean, but that the stochasticity can actually induce a qualitative difference in the shape of the conductance time series, namely, the presence or absence of a plateau period.

To obtain the data necessary to derive the desired conductance probability distribution, we take simulation data from 3 trials, each with $N = 60$ gap junctions. For each conductance time series, we set $t = 0$ to be the time at which the i^{th} cell is depolarized and proceed to collect conductance data for 32ms. This time normalization is done to eliminate correlation among the time series data and hence we are able to treat the conductance data for each gap junction as independent, greatly reducing the number of simulations needed to accumulate the data, as each simulation now will produce 299 independent realizations.

Since the source of stochasticity is modeled as Gaussian white noise, we can assume no auto-correlation within each time series data set. Thus, we are able to produce an unbiased estimator for the mean and the variance of the process from the sample mean and variance per time instance observation. We then have time-parametrized estimators for the mean and standard deviation that can be used to generate the normal probability distribution function for the time-dependent gap-junction conductance.

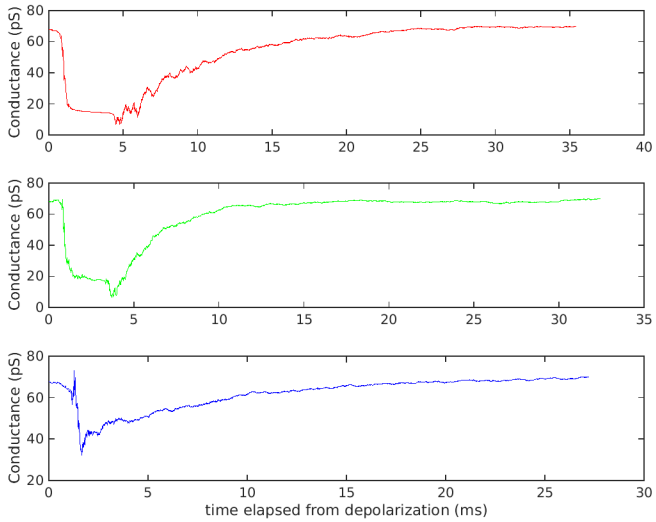

Figure 13: Time-series profiles for gap junction conductance data gathered from 3 simulation runs for the gap junction connecting cell 150 and 151. The model was run with $N = 60$ gap junctions. Time 0 refers to the time at which depolarization occurs in the cell at position 150 in the cable. Notice the drastically different conductance profiles between the top, middle and the bottom.

Figure 14 displays the time-dependent gap-junction conductance Gaussian probability surface. The large spread in the distribution for $t < 10$ms is a representation of the uncertainty in the process displaying conductance plateau behavior, as shown in Figure 13. The spread tightens as $t \to 32$ms as the conductance rises back to the pre-depolarization conductance distribution.

This distribution can be used as a characterization of model behavior as well as leveraged directly to generate samples of gap-junction conductance without the need to directly compute the model. Generating samples directly from the distribution can assist in the computationally efficient incorporation of stochastic gap-junction gating realized as gap-junction conductance, or equivalently, gap-junction resistance. Many larger-scale cardiac tissue models assume constant or deterministic gap-junction resistance [7], [11] to reduce computational requirements. Sampling techniques simulate stochastic elements with the advantage of not needing to compute them directly.

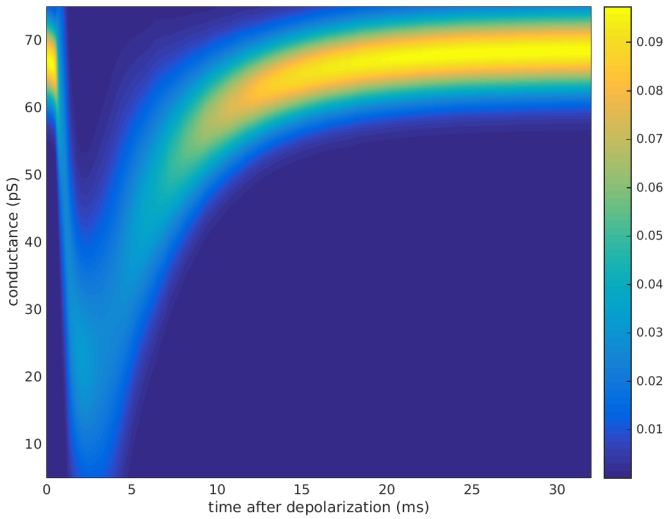

Figure 14: Gaussian probability surface describing the time-dependent gap-junction conductance distribution for the i^{th} gap junction. t_0 is taken to be the time of depolarization for the i^{th} cell. Notice the large spread in the distribution for $t < 10$ms. This is indicative of the uncertainty associated with the stochastic bifurcation realizations with and without the plateau in conductance. The spread tightens as $t \to 32$ as both forms return to the resting conductance distribution.

V. Discussion

In this section we discuss several ways to leverage the distributions derived in section IV. We begin by discussing situations in which sampling the distribution describing the process of interest can allow for the incorporation of stochastic effects into higher-level tissue simulations, at a reduced computational expense. We then shift our attention to validating model predictions via comparisons to experimental data, in particular, waiting-time distributions for single gap-junction gating-mode switches. We conclude the section by introducing some preliminary results on extending the use of stochastic differential equations to model CaRU gating.

V.1 Leveraging Distributions for Computational Efficiency

With a stochastic description of gap-junctional gating dynamics, both conduction block and conduction velocity in turn become stochastic processes, whose distributions were constructed in the previous section. These probabilistic representations can be leveraged in order simulate the effect of stochastic gap-junctional gating on macro-cardiac phenomena in a more computationally efficient manner.

Models used to investigate tissue-level phenomena, such as spiral-wave breakup, often employ minimalistic models of cellular current dynamics for computational feasibility [9], [7]. Action potential propagation can be modeled on a continuous domain, whereas cell-to-cell coupling is accomplished via a smoothing diffusion term, or on a discrete domain, where gap junctions are explicitly incorporated as local changes in resistance between cells [12]. Although it is known that gap-junction gating conformations alter the resistance between cells, and that gating conformations respond to both local voltage and local ionic concentrations and are inherently stochastic, these properties are often overlooked in tissue-level analysis, due in part to computational costs of simulating each gap-junction state individually.

We propose that gap-junction stochasticity can be efficiently incorporated into models by sampling the distributions constructed in analyzing the simulation data of our model. By initializing a desired number of gap junctions, N, coupling cells in a 1D, 2D, or 3D model of action potential propagation, stochastic gating effects can be incorporated by sampling from the appropriate N-indexed gap-junctional conductance (or resistance) distribution. That is, for a model with M gap junctions, M samples from a time-dependent gap-junction conductance distribution would be necessary at each time step. In contrast with solving M systems of SDEs at each time step or

even NM stochastic Markov simulations, computational and data storage demands are eased via sampling methods. If groups of cells are being simulated, stochastic conduction block and velocity can also be incorporated directly simply through sampling of the N-indexed conduction block or velocity distributions.

Emulator functions, such as the one constructed to estimate the binomial success parameter based on the number of gap junctions (see Figure 8), can also be constructed for the estimation of distribution parameters for conduction velocity, gap-junction current, and gap-junction conductance based on the number of gap junctions. Once such emulator functions are constructed, this technique allows for more rapid modeling over a larger number of gap junctions, as each change in N corresponds to an estimation of distribution parameters. This removes the necessity for a new computationally expensive Monte Carlo simulation for every value of N desired.

As stated, stochastic gating effects are most pronounced in the poorly coupled case, i.e., a reduced number of gap junctions. Such a reduction in the number of gap junctions (gap junction remodeling) is associated with many cardiac diseases that can induce arrhythmia and itself is considered to be arrhythmogenic [14]. Hence, these techniques would be useful when analysis of tissue-level propagation in such compromised physiological states is desired.

V.2 Waiting Time Distribution

The gating dynamics of gap junctions are stochastic processes of local voltage and ionic concentrations. The distributions associated with the length of time channels stay in the high-conducting state are referred to as dwell times. In [29], it was shown that a mouse connexin hemi-channel's dwell times follow an exponential distribution whose decay parameter increases with increasing voltage, as displayed in Figure 15. Since the more time a gap junction spends in the high conducting state, the more current is allowed to travel through to the adjacent cell, we expect the dwell times to be related to the wait-times defined in Section IV.3. As seen in Figures 11 and 12, the wait-time distributions in our model data conform well to a gamma distribution, with shape and scale parameters dependent upon the number of gap junctions.

Recall that wait times model the elapsed time between the maximum (in magnitude) gap-junctional current, I_j, of the gap junctions of two adjacent cells. Since the majority of the I_j results from the summation of gap junctions in the high-conducting state, whose dwell times in turn are exponential distributions, I_j is the summation of the current contributions of a set of exponentially distributed random variables and thus follows an Erlang distribution, which is a special case of

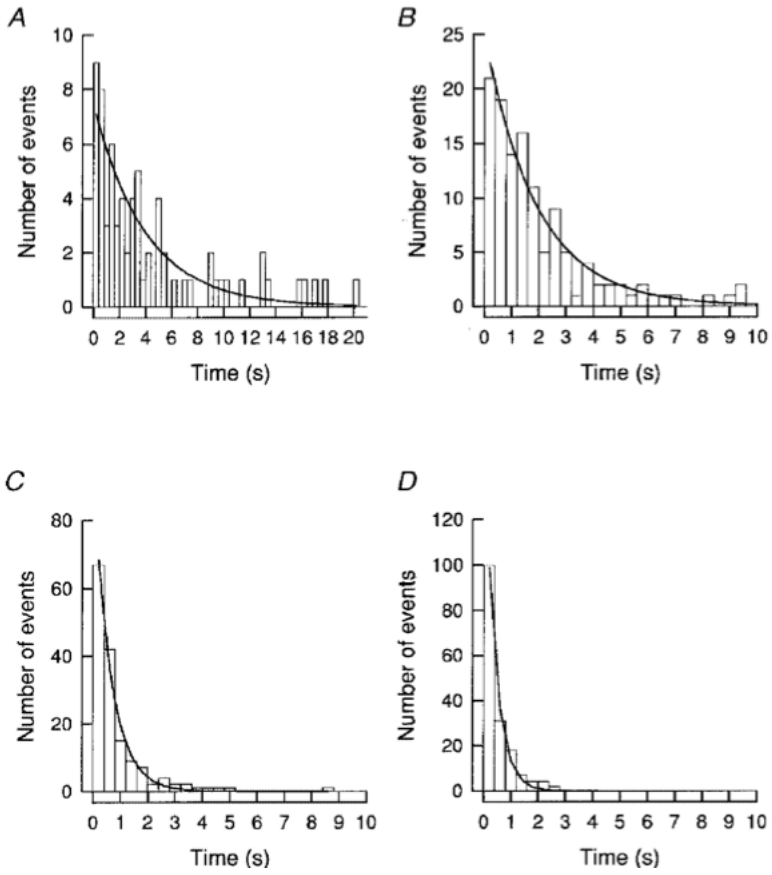

Figure 15: Experimental dwell time data for mouse gap junctions in the high-conducting state from [29]. Each panel records the number of gap junctions in the high-conducting state at each time observation. The curves represent best-fit exponential decay functions to the data. In panel A, the gap junction voltage V_j, was varied between 10 and 25mV. In B,C and D V_j was varied between 30 and 35mV, 40 and 45mV and 50 and 55mV respectively. Notice the decrease in the spread of the exponential distribution as the voltage is increased.

the gamma distribution. Therefore, the conformity of the wait-time data to a gamma distribution is to be expected based upon the underlying exponential distribution of experimentally measured dwell times.

V.3 Stochastic Calcium Gating

Intracellular calcium dynamics play a critical role in the initiation and regulation of the cardiac action potential. As mentioned, calcium-induded calcium release (CICR) is regulated by the gating of membrane L-type Ca^{2+} channels and RyR channels that line the Ca^{2+}-storing organelle, the sarcoplasmic reticulum. The gating modes of the L-type and RyR channels can be modeled as a single composite structure known as the calcium release unit (CaRU) [10]. Analogous to the gating dynamics of gap-junction channels, it known that the gating dynamics of L-type and RyR channels are inherently stochastic functions of the local Ca^{2+} concentration and membrane voltage.

In order to evaluate the probabilistic behavior of CaRU gating, we can apply the approach used throughout this thesis for modeling gap junctions to formulate a stochastic differential equation-based description of gating dynamics of collections of CaRUs from the deterministic description given in [13]. As in the gap-junction gating model, we are then able to define distributions for quantities or processes of interest. Here, we present preliminary results from efforts to determine the probabilistic behavior of the intracellular Ca^{2+} concentration from the contribution of a small number of CaRUs.

We devise a Monte Carlo-based scheme to generate data to estimate the time-dependent distribution for Ca^{2+}. The model was simulated for a total of 100 trials, each with a fixed number of 20 CaRUs. As in the gap-junction model, the system of stochastic differential equations describing gating dynamics was solved via an implementation of the Euler-Maruyama method while the ODEs used in the original model to describe the remaining cellular currents were integrated by the forward Euler method. The simulation was run for 500ms with a time step of $\Delta t = 0.01$ms. All model parameter values were taken to be those used in the original model formulation [13].

Figure 16 shows the parametric functional fits to the mean and variance of the Ca^{2+} concentration data gathered via the Monte Carlo simulation. The mean (top panel) was modeled as an exponential decay process, while the variance data was fit with a seventh-order interpolating polynomial. Fitting the variance data to both exponential and gamma distribution models was tested but ultimately discarded as neither could accurately capture enough of the variation in the data. Table

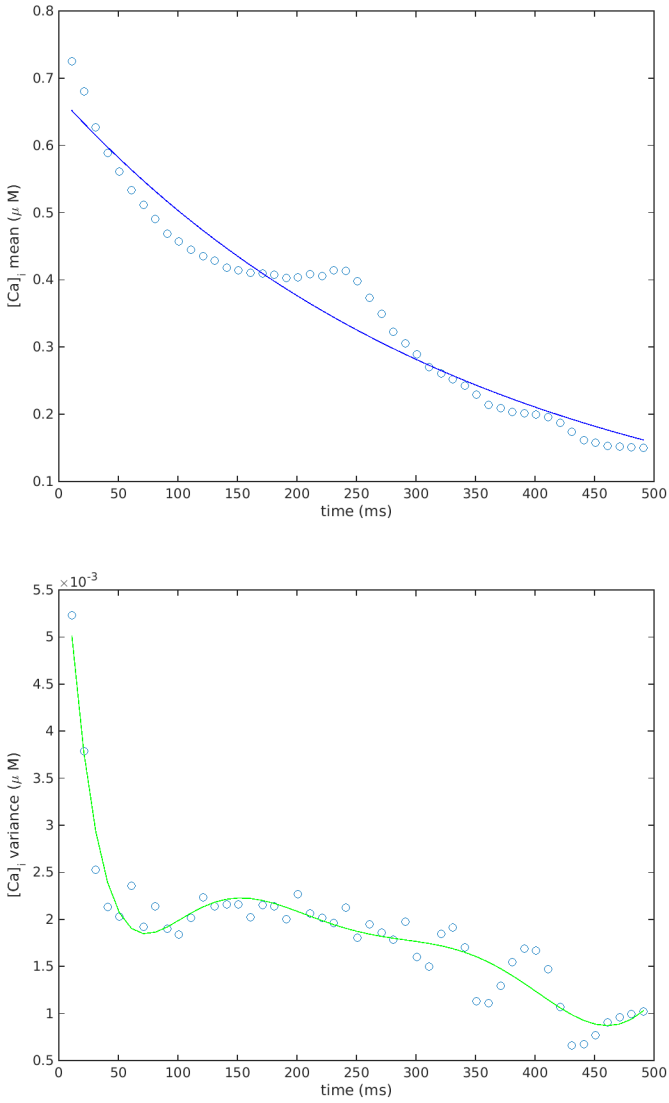

Figure 16: Fitting functional forms to the mean (top panel) and variance (bottom panel) of the time-dependent Ca^{2+} concentration data generated in Monte Carlo simulation. The model was simulated over 100 trials and the first two moments of the current data were computed. The mean data were fit with an exponential decay function, while the variance data were fit to an interpolating polynomial.

parameter model	r^2
$\sigma(t)$	0.92
$\mu(t)$	0.95

Table 7: r^2 statistic measuring what proportion of the variability in the data can be explained by each fit. The high coefficient of determination indicates a high level of explanatory ability for the mean and variance parametric models.

7 displays goodness-of-fit data for the time-dependent mean and variance functional fits. The values of the coefficient of determination indicate the fits explain over 90% of the variation from the data.

The stochasticity in the model results from idealized white noise, which suggests the resulting probability distribution of the gating currents is Gaussian [2]. Due to the independence of Wiener process samples used to integrate the SDE system, we assume there is no temporal covariance in Ca^{2+} concentration. Postulating a time-dependent Gaussian distribution with no covariance in either dimension, we may use the derived time-dependent parametric forms $\mu(t)$ and $\sigma(t)$ to approximate the time-dependent normal probability surface by using

$$p(Ca_i, \mu(t), \sigma(t)) = \frac{1}{\sigma(t)\sqrt{2\pi}} e^{-\frac{(Ca_i - \mu(t))^2}{2\sigma(t)^2}}. \tag{V.1}$$

Figure 17 shows a projection of the probability surface for Ca^{2+}. Notice that as the action potential progresses in time, the mean Ca^{2+} concentration decays and the variance of the process is reduced, visualized here as a tightening of the color gradient.

As with the probabilistic analysis of the stochastic gap-junction model, defining distributions for the intracellular Ca^{2+} concentration not only provides a probabilistic description of the model but also allows for the option of sampling from that distribution instead of computing the quantities directly, saving computational resources. The ability to sample distributions for stochastic model quantities leads to the possibility of more computationally efficient integration of stochastic subcellular currents into tissue level simulations. This will allow for more efficient analysis of subcellular stochasticity on tissue-level phenomenon. Ref. [24] simulates CaRU stochasticity on a 3D grid of 20,000 units and shows that such stochasticity can have an effect on the phase selection of action potential alternans (beat-to-beat irregularities in the action potential waveform) on the

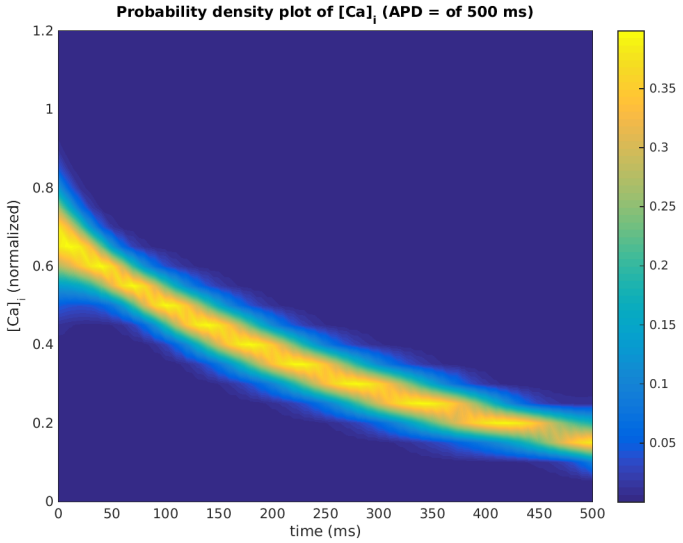

Figure 17: Gaussian probability surface for the time-dependent intracellular Ca^{2+} concentration. Fit functions were computed for mean and standard deviation data from the model simulation. The resulting time-dependent parametric forms were used to construct the probability surface.

cellular level, a macro-phenomenon. We propose that through characterizing the distribution of stochastically determined currents and sampling techniques, analysis of micro-structural stochasticity on macro-phenomena can be more efficiently scalable.

VI. Conclusion

In this thesis, we derived a novel stochastic-differential-equation-based description of gap-junction gating dynamics. Stochasticity in the form of Gaussian white noise was introduced to the deterministic formulation of gap-junction dynamics from Ref. [11] and we derived several distributions associated with model quantities of interest. Around the maximum number of gap junctions, N, for conduction block in the deterministic formulation, we determine a sigmoidal relationship between the probability, p, for no conduction block and N, with $p \to 1$ as $N \to \infty$ and $p \to 0$ as $N \to 0$. Conduction velocity on a 1D cable becomes a stationary stochastic process in our model, as it is a function of gap-junction resistance, and we determined the speed increases and variance decreases as N increases. We also use Monte Carlo simulation data to derive probability distributions modeling time-dependent maximum gap-junction current and time-dependent gap-junction conductance. The former is found to be a gamma distribution whereas the latter is modeled as a normal surface.

These derived distributions may be leveraged for incorporating stochastic effects via sampling techniques in larger, tissue-level cardiac simulations at a reduced computational cost. Further, we validated the modeling of time-dependent maximum gap-junction current as a gamma distribution via analysis of the summation of experimental gap-junction dwell-time data. We also introduced some preliminary results for the time-dependent distribution of intracellular Ca^{2+} concentration in a derived stochastic CaRU model.

One potential avenue of future work would be the implementation of stochastic gap-junction conductance into tissue-level bidomain models [7] via sampling distributions. The bidomain model allows such as an implementation as the inter-and intracellular dynamics are already formulated to be solved on separate domains. This could be an avenue to analyze stochastic effects on larger-scale tissue-level cardiac phenomena, such as spiral wave formation/breakup as well as phase selection in alternans [26]. Further, experimental data gathered on conduction block and velocity in tissue samples exhibiting poor cell-to-cell coupling (possibly in diseased state) could be of use in order to validate more of the distributions derived in the model. Statistical emulators, such as that modeled in Figure 8, could be derived for gap-junction ranges of interest over other distribution parameters for more rapid prototyping of samples.

In our model, we implement stochasticity in the form of Gaussian white noise in gating-mode dynamics. Although this may be an adequate approximation, stochasticity resulting from ionic concentration-based gating is largely overlooked in this study. Interesting extensions of this work

include extending the domain to simulate two- or three-dimensional tissue sections. In such regimes, the effect of stochastic gap-junction gating could be analyzed on emergent phenomena such as spiral wave (2D) and scroll wave (3D) breakup. The preliminary work presented on stochastic CaRU gating could be incorporated into 1D, 2D, or 3D tissue models as well, in which distributions could be derived for this source of stochasticity's effect on phase selection in sub-cellular alternans, as stochastic Ca^{2+} release has been indicated to have an effect on such processes [26].

VII. Acknowledgments

I would like to thank my thesis adviser Dr. Elizabeth Cherry as well as committee members Dr. Seshavandhani Kumar and Dr. Laura Munoz.

This work was supported in part by National Science Foundation grant number CMMI-1028261.

VIII. Bibliography

References

[1] American heart association. *Biotech Week*, page 22, Jan 28 2004. Name - American Heart Association; Copyright - Copyright 2004, Biotech Week via NewsRx.com NewsRx.net; Last updated - 2010-06-07.

[2] E. Allen. *Modeling with Itō stochastic differential equations*. Number v. 22 in Mathematical modelling–theory and applications. Springer, Dordrecht, 2007.

[3] Mostafa Bachar, Jerry J. Batzel, and Susanne Ditlevsen, editors. *Stochastic biomathematical models: with applications to neuronal modeling*. Number 2058 in Lecture notes in mathematics. Mathematical biosciences subseries. Springer, Heidelberg, 2013.

[4] G W Beeler and H Reuter. Reconstruction of the action potential of ventricular myocardial fibres. *The Journal of Physiology*, 268(1):177–210, June 1977.

[5] Jeremy M. Berg, John L. Tymoczko, Lubert Stryer, and Lubert Stryer. *Biochemistry*. W.H. Freeman, New York, 5th ed edition, 2002.

[6] L. Billard and P.W.A. Dayananda. A multi-stage compartmental model for HIV-infected individuals: Waiting time approach. *Mathematical Biosciences*, 249:92–101, March 2014.

[7] A. Bueno-Orovio, D. Kay, V. Grau, B. Rodriguez, and K. Burrage. Fractional diffusion models of cardiac electrical propagation: role of structural heterogeneity in dispersion of repolarization. *Journal of The Royal Society Interface*, 11(97):20140352–20140352, June 2014.

[8] F.F. Bukauskas and C. Peracchia. Two distinct gating mechanisms in gap junction channels: CO2-sensitive and voltage-sensitive. *Biophysical Journal*, 72(5):2137–2142, May 1997.

[9] Flavio H. Fenton, Elizabeth M. Cherry, Harold M. Hastings, and Steven J. Evans. Multiple mechanisms of spiral wave breakup in a model of cardiac electrical activity. *Chaos: An Interdisciplinary Journal of Nonlinear Science*, 12(3):852, 2002.

[10] Joseph L. Greenstein and Raimond L. Winslow. An Integrative Model of the Cardiac Ventricular Myocyte Incorporating Local Control of Ca2+ Release. *Biophysical Journal*, 83(6):2918–2945, December 2002.

[11] Alexandra P. Henriquez, Rolf Vogel, Barbara J. Muller-Borer, Craig S. Henriquez, Robert Weingart, and Wayne E. Cascio. Influence of Dynamic Gap Junction Resistance on Impulse Propagation in Ventricular Myocardium: A Computer Simulation Study. *Biophysical Journal*, 81(4):2112–2121, October 2001.

[12] C.S. Henriquez and A.A. Papazoglou. Using computer models to understand the roles of tissue structure and membrane dynamics in arrhythmogenesis. *Proceedings of the IEEE*, 84(3):334–354, March 1996.

[13] R. Hinch, J.L. Greenstein, A.J. Tanskanen, L. Xu, and R.L. Winslow. A Simplified Local Control Model of Calcium-Induced Calcium Release in Cardiac Ventricular Myocytes. *Biophysical Journal*, 87(6):3723–3736, December 2004.

[14] H. J. Jongsma and R. Wilders. Gap Junctions in Cardiovascular Disease. *Circulation Research*, 86(12):1193–1197, June 2000.

[15] M. Kohlmann. Stochastic differential equation: Oksendal B: An Introd. with Application. Springer-Verlag, Berlin, Heidelberg, New York, Tokyo 1985. *Metrika*, 33(1):246–246, December 1986.

[16] Joyce Lin and James P. Keener. Ephaptic Coupling in Cardiac Myocytes. *IEEE Transactions on Biomedical Engineering*, 60(2):576–582, February 2013.

[17] C. H. Luo and Y. Rudy. A model of the ventricular cardiac action potential. Depolarization, repolarization, and their interaction. *Circulation Research*, 68(6):1501–1526, June 1991.

[18] C. H. Luo and Y. Rudy. A dynamic model of the cardiac ventricular action potential. I. Simulations of ionic currents and concentration changes. *Circulation Research*, 74(6):1071–1096, June 1994.

[19] Y. Mori, G. I. Fishman, and C. S. Peskin. Ephaptic conduction in a cardiac strand model with 3d electrodiffusion. *Proceedings of the National Academy of Sciences*, 105(17):6463–6468, April 2008.

[20] D. Noble. A modification of the Hodgkin–Huxley equations applicable to Purkinje fibre action and pace-maker potentials. *The Journal of Physiology*, 160:317–352, February 1962.

[21] Nerijus Paulauskas, Henrikas Pranevicius, Jonas Mockus, and Feliksas Bukauskas. Stochastic 16-State Model of Voltage Gating of Gap-Junction Channels Enclosing Fast and Slow Gates. *Biophysical Journal*, 102(11):2471–2480, June 2012.

[22] Nerijus Paulauskas, Mindaugas Pranevicius, Henrikas Pranevicius, and Feliksas F. Bukauskas. A Stochastic Four-State Model of Contingent Gating of Gap Junction Channels Containing Two Fast Gates Sensitive to Transjunctional Voltage. *Biophysical Journal*, 96(10):3936–3948, May 2009.

[23] Serguei Primak, V. IA Kontorovich, and Vladimir Lyandres. *Stochastic methods and their applications to communications stochastic differential equations approach*. Wiley, Chichester; Hoboken, NJ, 2004.

[24] Juan G. Restrepo and Alain Karma. Spatiotemporal intracellular calcium dynamics during cardiac alternans. *Chaos: An Interdisciplinary Journal of Nonlinear Science*, 19(3):037115, 2009.

[25] J. J. Rice, M. S. Jafri, and R. L. Winslow. Modeling gain and gradedness of Ca2+ release in the functional unit of the cardiac diadic space. *Biophysical Journal*, 77(4):1871–1884, October 1999.

[26] Daisuke Sato, Donald M. Bers, and Yohannes Shiferaw. Formation of Spatially Discordant Alternans Due to Fluctuations and Diffusion of Calcium. *PLoS ONE*, 8(12):e85365, December 2013.

[27] Timothy Sauer. Numerical Solution of Stochastic Differential Equations in Finance. In Jin-Chuan Duan, Wolfgang Karl Härdle, and James E. Gentle, editors, *Handbook of Computational Finance*, pages 529–550. Springer Berlin Heidelberg, Berlin, Heidelberg, 2012.

[28] Y. Shiferaw, M.A. Watanabe, A. Garfinkel, J.N. Weiss, and A. Karma. Model of Intracellular Calcium Cycling in Ventricular Myocytes. *Biophysical Journal*, 85(6):3666–3686, December 2003.

[29] Virginijus Valiunas, Dieter Manthey, Rolf Vogel, Klaus Willecke, and Robert Weingart. Biophysical properties of mouse connexin30 gap junction channels studied in transfected human HeLa cells. *The Journal of Physiology*, 519(3):631–644, September 1999.

[30] Rolf Vogel and Robert Weingart. Mathematical model of vertebrate gap junctions derived from electrical measurements on homotypic and heterotypic channels. *The Journal of Physiology*, 510(1):177–189, July 1998.

[31] George S.B. Williams, Marco A. Huertas, Eric A. Sobie, M. Saleet Jafri, and Gregory D. Smith. A Probability Density Approach to Modeling Local Control of Calcium-Induced Calcium Release in Cardiac Myocytes. *Biophysical Journal*, 92(7):2311–2328, April 2007.

[32] Raimond L. Winslow, Sonia Cortassa, Brian O'Rourke, Yasmin L. Hashambhoy, John Jeremy Rice, and Joseph L. Greenstein. Integrative modeling of the cardiac ventricular myocyte. *Wiley Interdisciplinary Reviews: Systems Biology and Medicine*, 3(4):392–413, July 2011.